Case Studies in Thermal Engineering 30 (2022) 101761

Contents lists available at ScienceDirect

Case Studies in Thermal Engineering

journal homepage: www.elsevier.com/locate/csite

A comparison of the pulsating and steady jets on flow-induced vibrations and thermal behavior of a sprung cylinder inside an isothermal channel

S.D. Farahani [a], A.H. Rabiee [a,*], A.M. Zakinia [a], Amir Mosavi [b,c,d,**]

[a] School of Mechanical Engineering, Arak University of Technology, Arak, Iran
[b] John von Neumann Faculty of Informatics, Obuda University, 1034 Budapest, Hungary
[c] Institute of Information Engineering, Automation and Mathematics, Slovak University of Technology in Bratislava, Slovakia
[d] Institute of Information Society, University of Public Service, 1083 Budapest, Hungary

ARTICLE INFO

Keywords:
Flow-induced vibrations
Pulsating and steady jet
Isothermal channel
Heat transfer
Frequency response
Vortex shedding

ABSTRACT

In this paper, the effect of the pulsating jet from channel walls on the thermal and vibrational behavior of the elastically-mounted cylinder is examined. For the sake of comparison, the efficiency of the steady jet in which the injection velocity is constant has also been taken into account. The primary parameters studied are jet distance, pulsating jet velocity, and frequency. The finite volume method is used to solve flow and energy equations. The dynamic mesh approach is also utilized for the cylinder's motion coupling with a flow field. The results of fluid-solid interaction simulations demonstrate that the pulsating jet acts very successfully in reducing cylinder vibrations, so that at $U_j = 2$, The maximum cylinder displacement magnitude is reduced by 91%, 94%, and 94% for slots 1, 2, and 3, respectively. On the other hand, to reduce the cylinder displacement by the steady jet, the injection velocity must be large enough in which the efficiency decreases significantly as the jet distance increases. The primary reason for the vibration reduction in the steady jet is to suppress the vortex shedding behind a circular cylinder. However, as the jet distance increases, the ability of the steady jet to make changes to vortices decreases, and for this reason, no significant difference in the cylinder displacement magnitude is observed for slot 3. In contrast, the main mechanism for reducing vibrations in a pulsating jet is to change the vortex shedding frequency. Consequently, the cylinder comes out the lock-in region, and the displacement magnitude is reduced independently of jet injection from triple slots.

1. Introduction

Intermittent vortex shedding from rigid structures results in the application of alternating dynamic forces and, consequently, vibrations or acoustic noise may occur [1,2]. The resulting motion is known as vortex-induced vibrations, which in the lock-in region (matching the vortex-induced frequency with the natural frequency of bluff body) can lead to irreparable damages to many structures, such as heat exchanger pipes, risers, offshore platforms, pipeline transport, tall buildings and so on [3–5]. Hence, reducing such vibrations by various VIV control methods has been the objective of much research in recent decades. From one viewpoint, VIV reduction methods are divided into flow control and direct vibrational control methods, the first of which is VIV reduced by changes in the vortex

* Corresponding author.
** Corresponding author.
E-mail addresses: rabiee@arakut.ac.ir (A.H. Rabiee), amir.mosavi@kvk.uni-obuda.hu (A. Mosavi).

https://doi.org/10.1016/j.csite.2022.101761
Received 12 November 2021; Received in revised form 1 January 2022; Accepted 4 January 2022
Available online 5 January 2022

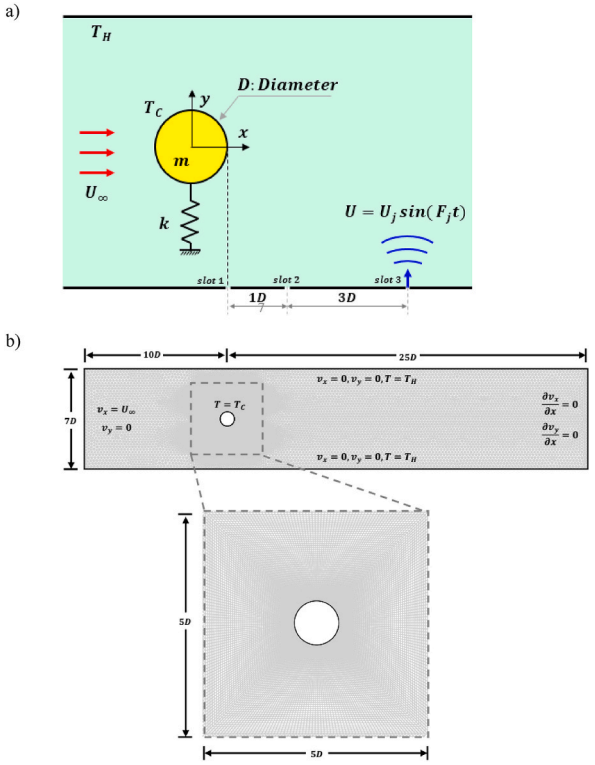

Fig. 1. a) Physical model schematic of a problem and jet injection site, and b) cylindrical general view located in a channel, meshing and boundary conditions.

shedding process or make an impact on the bluff body wake that consequently the dynamic forces from the fluid to structure suppressed [6,7]. In direct vibrational control methods, the VIV reduction is targeted directly by various control actuators [8,9]. From another viewpoint, VIV reduction methods are classified into passive and active control techniques. Passive methods act mainly with changes in bluff body geometry, without the need for an external energy source [10,11]. Although passive methods are easier to implement and also do not require external energy, they are effective within a certain range, and in some cases, can even increase VIV. In contrast, active methods are more effective in reducing VIV by utilizing power from an external energy source [12,13]. Using jet or flow blowing is one of the active flow control methods (flow control from the first category + active control from the second category), which has successfully been able to modify the flow around a cylinder, reduce lift and drag coefficients and subsequently reduce cylinder VIV.

Williams et al. [14], for example, succeeded in practically reducing VIV by injecting jets through holes in the cylinder surface. With experiments performed in a water channel, Feng and Wang [15] succeeded in reducing the interactions between separated upper and lower vortices by using jet injection from a slot created at the rear stagnation point, and consequently reducing forces acting on it. In another work, Feng and Wang [16] also studied the effect of jet synthesis from the front stagnation point of the cylinder on the vortical structure. Dong et al. [17] tested a new control method by combining flow suction from the front surface of the cylinder and blowing the same flow from the rear surface of the cylinder, they succeeded in significantly reducing the lift coefficient magnitude. They showed that simultaneous suction and blowing were more effective than suction or blowing alone. Chen et al. [18] reduced the lift and drag coefficients magnitude of a circular cylinder, both experimentally and numerically, by creating a groove between the front and rear stagnation points. Recently, Wang, et al. [19] investigated numerically the influence of pulsating jet angle and its phase difference on the cylinder VIV. They showed that the jet angle is a significant parameter that, if not chosen correctly, can even increase the VIV magnitude.

Another interest of researchers in recent years has been to address the thermal characteristics of stationary or vibrating cylinders [20,21]. However, most of this research has been focused on heat transfer from stationary cylinders, which can be referred to as the cylinder geometry and inlet flow characteristics [22]. For example, Kumar, et al. [23] studied the heat transfer and flow field around a semi-circular cylinder with a circular cylinder. They showed that the drag coefficient of a semi-circular cylinder was higher than that of a circular one. It was also observed that the average Nusselt number of semi-circular cylinders rises with increasing Reynolds number and Prandtl number. Sharma et al. [24] found that there was a connection between the wake length and the average Nusselt number of a square cylinder, so that as the wake length increases, so does the average Nusselt number, and both increase with increasing Reynolds number. Dhiman and Hasan [25] studied the heat transfer and flow around a cylinder with a trapezoidal cross-section and found that the heat transfer coefficient was higher for this cylinder and its drag coefficient was lower. In another work, Dhiman [26] examined the flow field characteristics and heat transfer of a triangular cylinder and showed that the blockage ratio has an important effect on the

heat transfer. Chatterjee and Amiroudine [27] studied the heat transfer of tandem square cylinders and found that heat transfer and drag coefficient increased with increasing the blockage ratio.

There is limited research conducted mainly in recent years on the study of heat transfer from vibrational bluff bodies. The combination of VIV problem and heat transfer is inevitable in some engineering applications such as heat exchanger pipes. Lin et al. [28] showed that the heat transfer from a vibrational bluff body in the Lock-in range increases by 13%. Su et al. [29] studied the VIV and heat transfer of circular, vertical, and horizontal ellipse cylinders and found that the vertical one has a higher displacement amplitude as well as a higher heat transfer rate than the other two geometries. Izadpanah et al. [30] examined the heat transfer and the one degree of freedom VIV of a circular cylinder. They showed that with increasing velocity, the average Nusselt number first rises and then decreases. Recently, Yang, et al. [31] studied heat transfer and VIV of a circular cylinder that vibrates freely in in-line and cross-flow directions. They showed that the two degrees of freedom VIV could increase the average Nusselt number by 2.46% relative to the vibrational cylinder of one degree of freedom.

According to a review of the conducted research, it is observed that although many researches have been done on VIV control through jet injection, stationary cylinder heat transfer with different geometries, and also heat transfer of vibrational cylinders, the influence of jet flow from channel walls is not done on heat transfer and VIV. For this purpose, in the first step, we studied the effect of steady jet injection on the displacement magnitude, and thermal behavior of cylinder vibrated freely in the cross-flow direction [32]. In the second step, in this study, our aim is to study the effect of pulsating jet parameters on the lift and drag coefficients, displacement, and heat transfer of a flexibly supported circular cylinder inside a channel. For this purpose, the pulsating jet magnitude and frequency from three different slots located at distances $L/D = 0, 1,$ and 4 from the cylinder center have been considered.

2. Physical model

In this study, the effect of the pulsating jet from the lower wall of a channel on free transverse vibration and heat transfer of circular cylinder positioned in the isothermal channel was examined numerically. The intended problem is shown in Fig. 1a. The cylinder can oscillate freely in the y-direction. Slots are located on the lower wall of the channel at intervals of $L/D = 0, 1,$ and 4 from the cylinder center. The nearest slot to the cylinder is slot 1, which is located precisely at the bottom right of the cylinder. The second slot is 1D away from the first one and the third slot has the longest distance and is located at a 3D distance from the second slot.

3. Governing equations

Assuming Newtonian fluid, continuity, momentum, and energy for flow equations in the channel are expressed as follows:

$$\nabla.V = 0 \tag{1}$$

$$\rho\frac{D\vec{V}}{Dt} = -\nabla P + \mu\nabla^2\vec{V} \quad \frac{D\vec{V}}{Dt} = \frac{\partial\vec{V}}{\partial t} + \vec{V}.\nabla\vec{V} \tag{2}$$

$$\rho c_p\left(\frac{\partial T}{\partial t} + \vec{V}.\nabla T\right) = \nabla.(\lambda\nabla T) \tag{3}$$

which T, ρ, P, t, μ, V, C_P, and λ are temperature, fluid density, static pressure, time, dynamic viscosity, velocity, heat capacity at constant pressure, and thermal conductivity coefficient. Temporal changes of the pulsating jet outlet velocity from the slot on the channel wall are considered as follows:

$$U = U_j\sin(F_j t) \tag{4}$$

where U_j and F_j are defined as follows:

$$U_j = \frac{Vj}{U_\infty} \tag{5}$$

$$F_j = \frac{2\pi f_j}{\sqrt{k/m}} \tag{6}$$

Where V_j is the jet velocity, U_∞ is the inlet flow velocity to the channel, f_j is the jet oscillation frequency, k is the spring stiffness coefficient, and m is the body mass. The boundary conditions are shown in Fig. 1b. For channel walls and cylinders, the no-slip boundary condition is used. Channel and cylinder wall temperatures are considered T_H and T_c, respectively. The fluid enters the channel with uniform velocity and temperature U_∞ *and* T_∞. The Outlet boundary condition is considered for the right vertical boundary of the solution domain. The pulsating jet is injected into the channel from the intended slots on the lower wall of the channel with velocity and temperature T_∞ and U_j. When a circular cylinder is exposed to a uniform flow, the vortices are shed symmetrically and alternately, which causes oscillating forces from the fluid to the cylinder. If the cylinder is placed on a flexible subgrade, as shown in Fig. 1a, it will start vibrating due to oscillating forces exerted by the fluid. Here, the cylinder motion in the y-direction is limited, known as cross-flow or transverse displacement. To model a vibrational motion, it is assumed that the cylinder with mass m is connected to a spring with a hardness of k and a damper with a damping factor of c in the y-direction. Therefore, the classical second-order equation can be used as follows:

Table 1
Mean drag and maximum lift coefficients of the circular cylinder at Re = 100 for different grid sizes.

	Total no. of cells	No. of cells in the central block	$\overline{C}_D$	C_L^{max}
Case 1	8900	3000	1.45	0.42
Case 2	15600	5000	1.43	0.41
Case 3	17000	7000	1.42	0.4
Case 4	**21000**	**7000**	**1.39**	**0.38**
Case 5	61400	9000	1.385	0.376

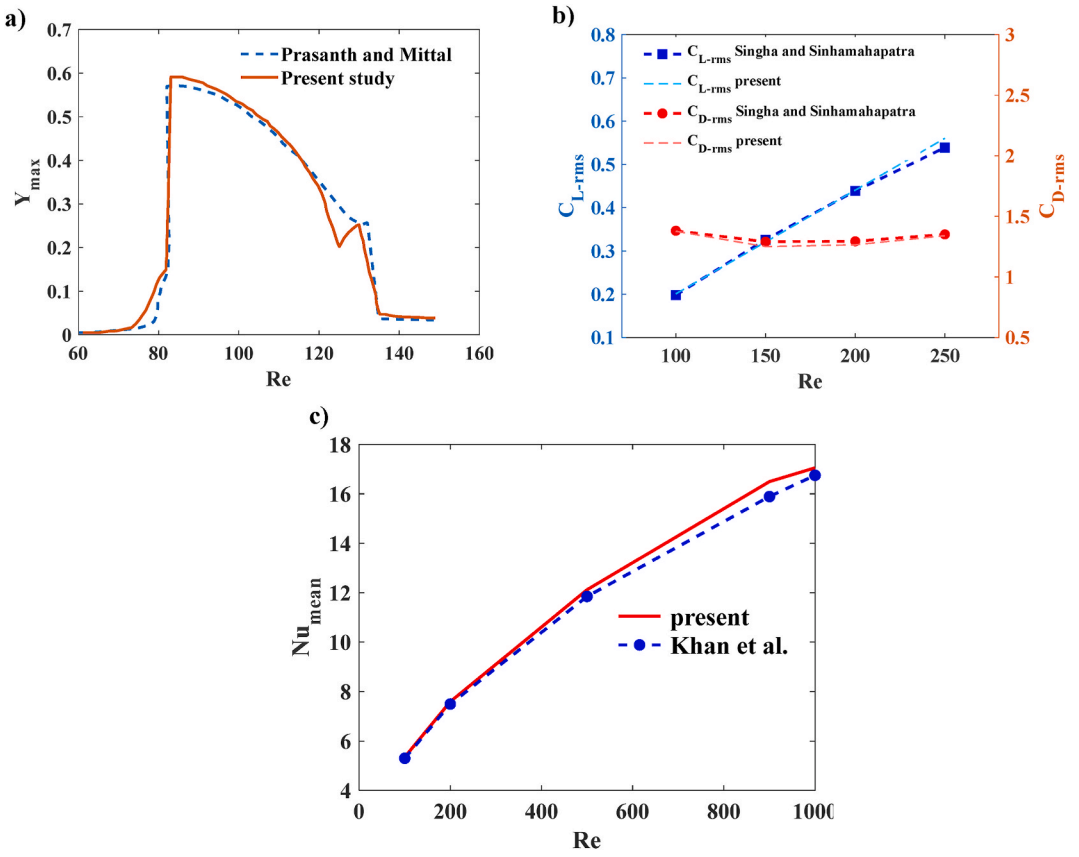

Fig. 2. Validation of results a) maximum displacement changes in terms of Reynolds number, b) root mean square changes in lift and drag coefficients in terms of Reynolds number, and c) the average Nusselt number changes in terms of Reynolds.

$$m\ddot{y} = -c\dot{y} - ky + f_L \tag{7}$$

Where f_L is the lift force, y is the cross-flow displacement, $\dot{y}$ and $\ddot{y}$ are the first- and second-time derivatives of y, which are the same as cross-flow velocity and acceleration, respectively. Knowing the Reynolds number $\mathrm{Re} = \rho U_\infty D/\mu$ and the dimensionless mass $m^* = 4m/(\pi\rho D^2)$ as well as the dimensionless natural frequency $f_n^* = (\frac{D}{2\pi U_\infty})\sqrt{k/m}$, the parameters of equation (7) are calculated. The drag and lift coefficients, are defined as:

$$C_D = f_D/(0.5\rho U^2 D) \tag{8}$$

$$C_L = f_L/(0.5\rho U^2 D) \tag{9}$$

where f_D is the drag force. To maximize the cylinder vibration magnitude, the damping value equals zero. Also, the Nusselt number is defined according to equation (10).

$$Nu = -\frac{D\frac{\partial T}{\partial y}|y=0}{T_H - T_m} \tag{10}$$

T_m is the average fluid temperature.

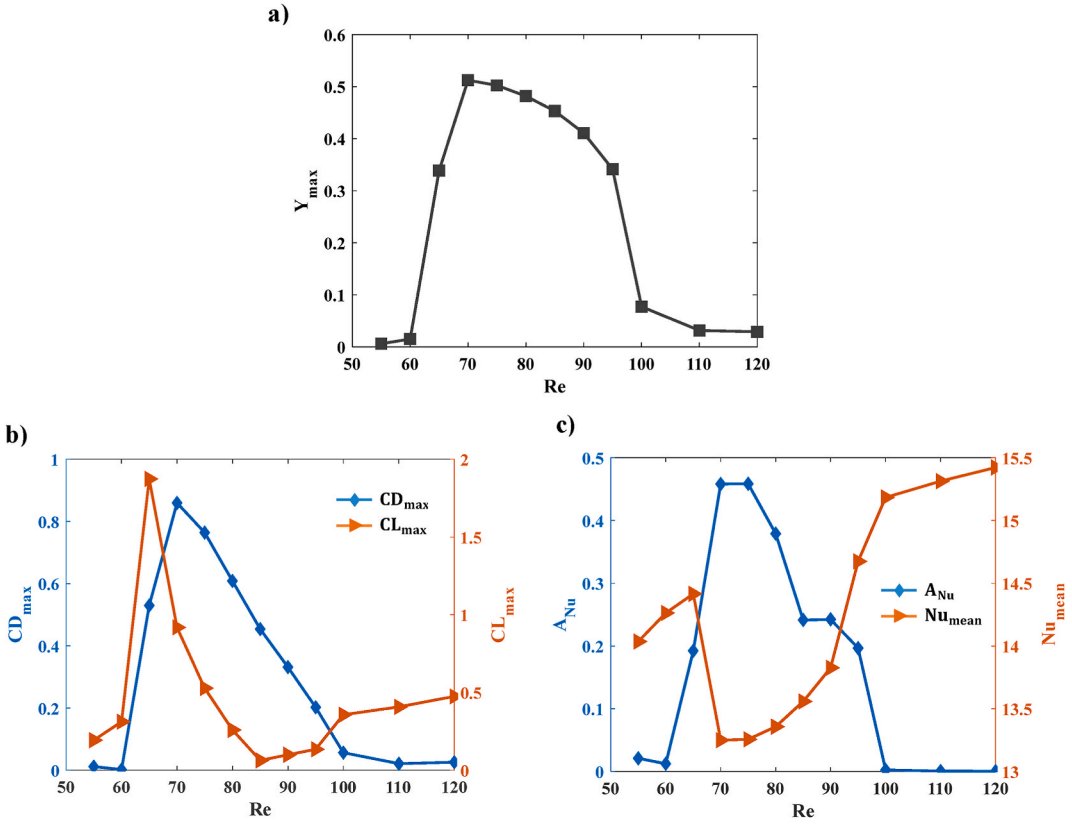

Fig. 3. The change in a) maximum displacement, b) lift and drag coefficients, and c) amplitude and the average of Nusselt number, for uncontrolled cylinders in terms of Reynolds number.

4. Numerical solution method

During the transient solution, lift and drag coefficients on a cylinder are computed by the finite volume method with a programming language. These aerodynamic forces are loaded by User-Defined Function (UDF) for ANSYS Fluent software. Using it, the resulting force value exerted by the damper, spring, and flow is calculated, then the body acceleration and the motion velocity in the solution time interval are achieved. The PISO method is used to solve velocity-pressure coupling, the Presto! method is used to discretize the pressure gradient, and the Quick method is utilized to discretize momentum equations. It is required that the computational domain is meshed for the numerical solution. Dynamic mesh is used to simulate the cylinder motion. It is very important to choose the right mesh size to get accurate results. Here, to examine the influence of grid size on the results obtained, the general grid shape is preserved while the mesh size is reviewed in three different modes. For this purpose, the maximum drag and lift coefficient of a fixed cylinder in Re = 100 is obtained for multiple grids, and the results are shown in Table 1. The results show that case 4 is a good choice to continue the reviews. Medium mesh size is a good choice for upcoming simulations. This grid has established a good compromise between the accuracy of results and the computational cost. Fig. 1b shows the intended problem mesh.

At this point, it is required to examine the validity of the presented numerical modeling. For this purpose, the values of inlet parameters are considered as $f_n^* = 16.4/\mathrm{Re}$, $B = 0.05$, $\zeta = 0$, and $m^* = 10$ so that the vibrations of 2 DOF of a cylinder are expressed in terms of Reynolds number. Fig. 2a shows that these results match well with the numerical space-time method results driven by Prasanth and Mittal [33]. The mean value of drag coefficient, and the RMS of lift coefficient for a cylinder within the channel in the range of $200 < Re < 250$ are checked with the outcomes of Singha and Sinhamahapatra [34]. Fig. 2b displays that the results are in good matching with Singha and Sinhamahapatra [34] numerical outputs. Next, the heat transfer coefficient in the range of $200 < Re < 2000$ is calculated for a fluid with a Prandtl number of 0.7 and, as shown in Fig. 2c, is consistent with the results of Khan et al. [35].

5. Numerical results

In this section, the resultsl of fluid-solid interaction simulations are presented. First, the effect of pulsating and steady jet on the maximum cylinder displacement magnitude, lift, and drag coefficients, as well as Nusselt number have been reviewed. Then vorticity and temperature contours for the pulsating jet are examined from different slots. In the following, the effect of pulsating jet frequency on the results is given. Finally, using frequency response diagrams, the main mechanisms of VIV reduction by the steady and pulsating jet are discussed.

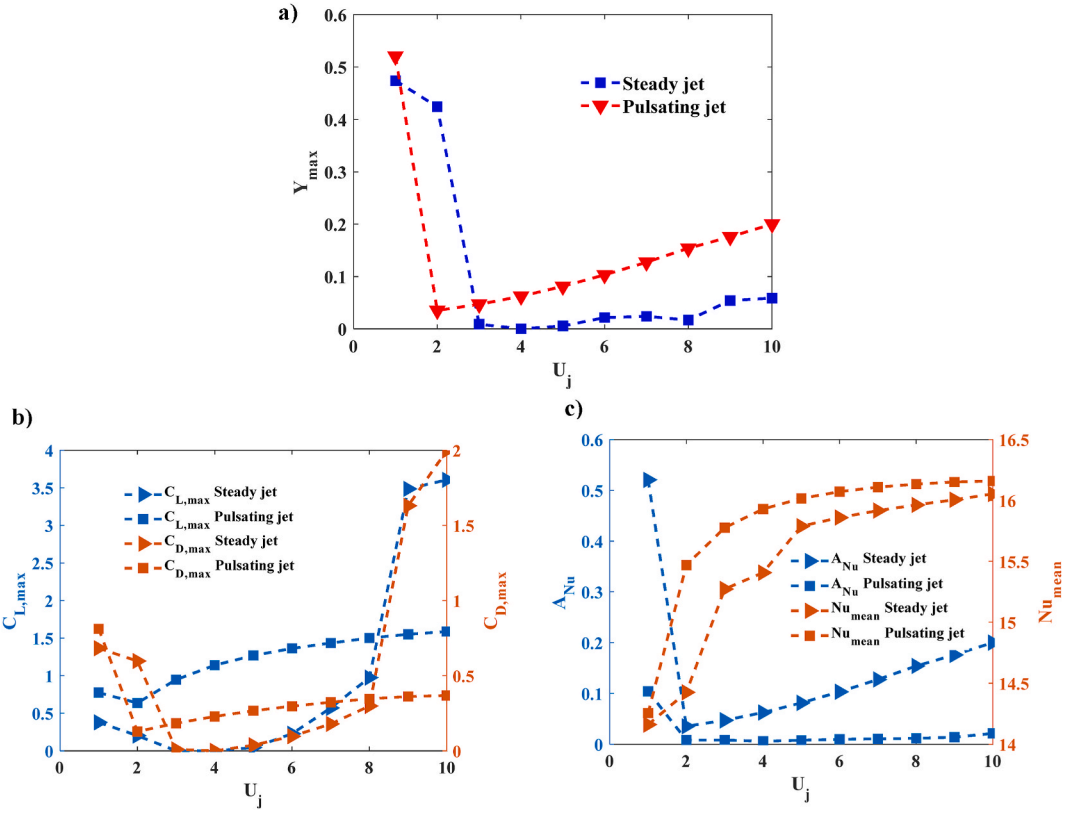

Fig. 4. Changes in the cylinder response for steady and pulsating jet injection from slot 1 in terms of flow injection velocity a) Maximum displacement, b) Maximum lift and drag coefficients, and c) Amplitude and the average of Nusselt number.

Fig. 3a shows the change in maximum displacement of the cylinder located in the channel with a height of 7*D* in terms of Reynolds number. Also, in Fig. 3b, the maximum of lift and drag coefficients magnitude, as well as the maximum average Nusselt number are given. It can be seen that as the Reynolds number increases, the displacement increases abruptly due to the frequency matching in the lock-in region. In this regard, the transverse displacement at $Re = 70$ has reached its maximum value ($Y_{max} = 0.52$). Frequency matching transfers energy from the fluid to structure and consequently increases the hydrodynamic coefficients, as shown in Fig. 3b. As it can be seen from Fig. 3c, the changes of Nusselt number amplitude increase and then decrease with increasing Reynolds number, reaching its maximum value in Re = 70.

The behavior of Nusselt number amplitude in terms of Reynolds number is almost similar to the changes in cylinder transverse displacement. Changes in the average Nusselt number with Reynolds have observed a minimum value in Re = 70. This minimum is due to the change in frequency of vortices generated behind the cylinder and frequency matching that causes some of the fluid energy to be transferred to the structure. After Reynolds number of 70, with the increase of Reynolds, the average Nusselt number increases with the rise in vortices created behind the cylinder. Given that the maximum cylinder displacement amplitude occurs around $Re = 70$, the continued results for this Reynolds number are given below.

Fig. 4a shows the maximum transverse displacement of a circular cylinder in terms of the pulsating jet velocity for slot 1 with a frequency ratio of $F_j = 1$ at $Re = 70$. Steady jet results are also shown for comparison. It can be seen that the motion magnitude decreases abruptly from $U_j = 2$ while the same value for the steady jet is $U_j = 3$. In particular, the displacement magnitude for the pulsating jet at $U_j = 2$ and the steady jet at $U_j = 3$ decreased by 91% and 97%, respectively. Afterward, with increasing the velocity amplitude, a slight increase is seen in displacement for both steady and pulsating jets.

In the following, Fig. 4b shows the maximum lift and drag coefficients in terms of steady and pulsating jet velocity. Here, the changes in coefficients are almost identical to displacement variations: a significant decrease with increasing jet velocity and then an increase, especially for the steady jet. Fig. 4c shows the amplitude and average of the Nusselt number in terms of the steady and pulsating jet velocity. The changes of Nusselt number amplitude in both steady and pulsating jet cases decrease with increasing jet velocity. Nusselt number variation seems to be a function of velocity and temperature changes.

Therefore, by reducing transverse vibrations, the created oscillations in the velocity and temperature fields are reduced, and consequently, Nusselt number oscillations are also reduced. The Nusselt number amplitude in the steady jet is greater than the pulsating jet. The average Nusselt number increases with increasing the pulsating and steady jet velocity. The Nusselt number in the pulsating jet is more than the steady one. The reason for this thermal behavior is that when the jet is injected from a channel wall, it destroys the hydrodynamic and thermal boundary layer formed on the channel wall, and a part of fluid near the wall, which is hot

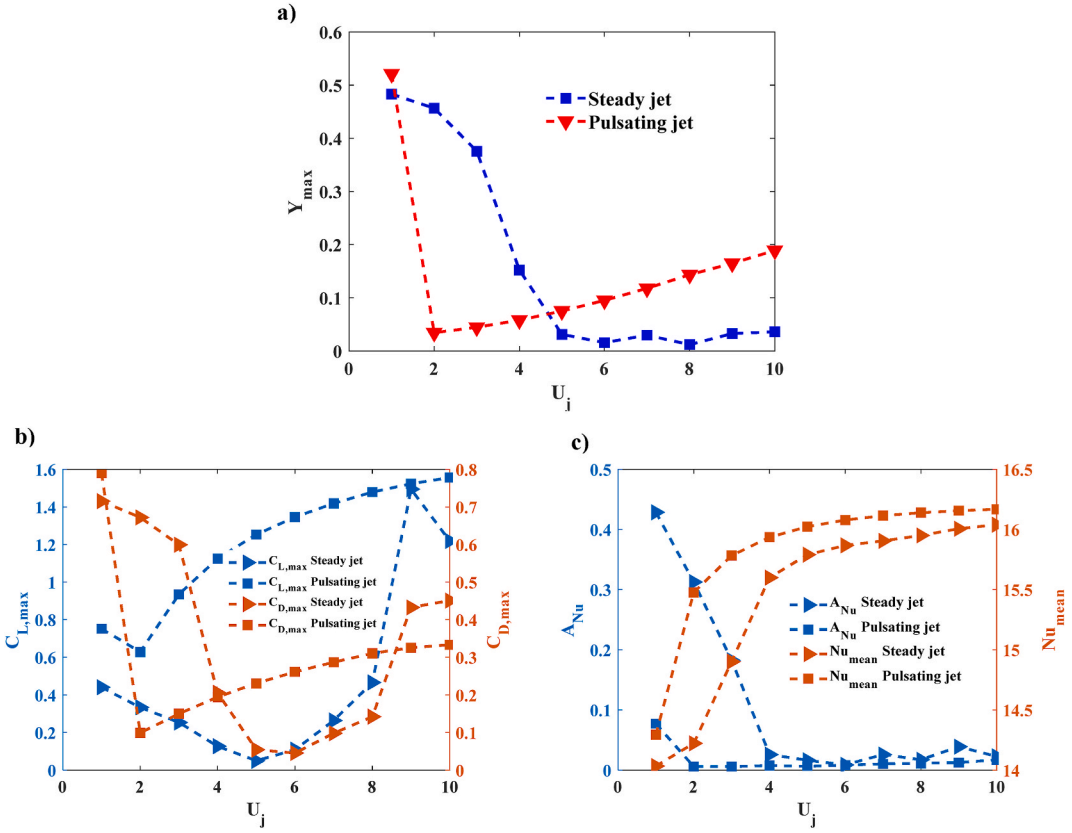

Fig. 5. Changes in the cylinder response for steady and pulsating jet injection from slot 2 in terms of flow injection velocity: a) Maximum displacement, b) Maximum lift and drag coefficients, and c) Amplitude and the average of Nusselt number.

fluid, is thrown towards the channel center, leading to the increased disturbance and mixing, and increases the average temperature of fluid behind the cylinder. When the jet velocity changes with time (pulsating jet), the hydrodynamic boundary layer on the lower wall is destroyed periodically, which further increases disturbances behind the cylinder, and the positive effect of jet on increasing the heat transfer coefficient are more.

Fig. 5 shows the identical results as Fig. 4, this time for slot 2, which is further away from the cylinder. Here, the turning point, where a sudden decrease in displacement magnitude occurs, is seen for the steady jet at $U_j = 5$. At this velocity, the displacement response to the uncontrolled cylinder is reduced by 95%. Surprisingly, it can be seen that the effectiveness of pulsating jet for slot 2 has not changed compared to slot 1. For a pulsating jet, vibrations reduction still starts from $U_j = 2$. In this jet velocity, the maximum displacement magnitude decreased by 94.7%. The trend of changes in lift and drag coefficients for slot 2 is the same as before, with the difference that the increase rate of these coefficients with increasing the velocity for steady and pulsating jets is less than slot 1. Changes in the Nusselt number amplitude associated with slot 2 are similar to that of slot 1, with the difference that at $U_j = 4$, a sudden decrease has occurred. The changes in the average Nusselt number of slot 2 are almost similar to that of slot 1.

In the following, Fig. 6 shows the displacement variations, lift and drag coefficients, and the Nusselt number characteristics for steady and pulsating jet for slot 3, which is the farthest from the cylinder relative to other slots. Here, it can be seen that the steady jet did not have a significant effect on the displacement response, while the pulsating jet was able to maintain its efficiency in reducing the cylinder displacement. In particular, the pulsating jet with domain $U_j = 2$ reduced the cylinder displacement amplitude by 94%.

Also, the lift and drag coefficients for steady jet did not change significantly for velocity change. The Nusselt number amplitude changes in the pulsating jet for slot 3 are the same as the other two slots. But in the steady jet, unlike the previous two states, no sudden drop is observed in the Nusselt number. This may be due to the jet injection position distance from the cylinder and the diminishing effect of the jet on vortex shedding behind the cylinder and transverse oscillations. The average Nusselt number variations in the pulsating and steady jets are similar to the two slots 1 and 2, and they increase with increasing injection velocity. It can be seen that with growing jet injection velocity from 5 onwards, the difference between the average of Nusselt number in pulsating and steady jets has decreased very little.

Fig. 7a shows vorticity contours associated with different pulsating jet velocities for all slots 1, 2, and 3. It can be seen that the vortical structure for all velocities is the same as the uncontrolled cylinder (2S mode). In this mode, one vortex from the top and the other one from the bottom is shed periodically. As the velocity increases, not much change is seen in the cylinder wake. Fig. 7b shows temperature contours associated with different pulsating jet velocities for all slots 1, 2, and 3. As the velocity increases, it is observed

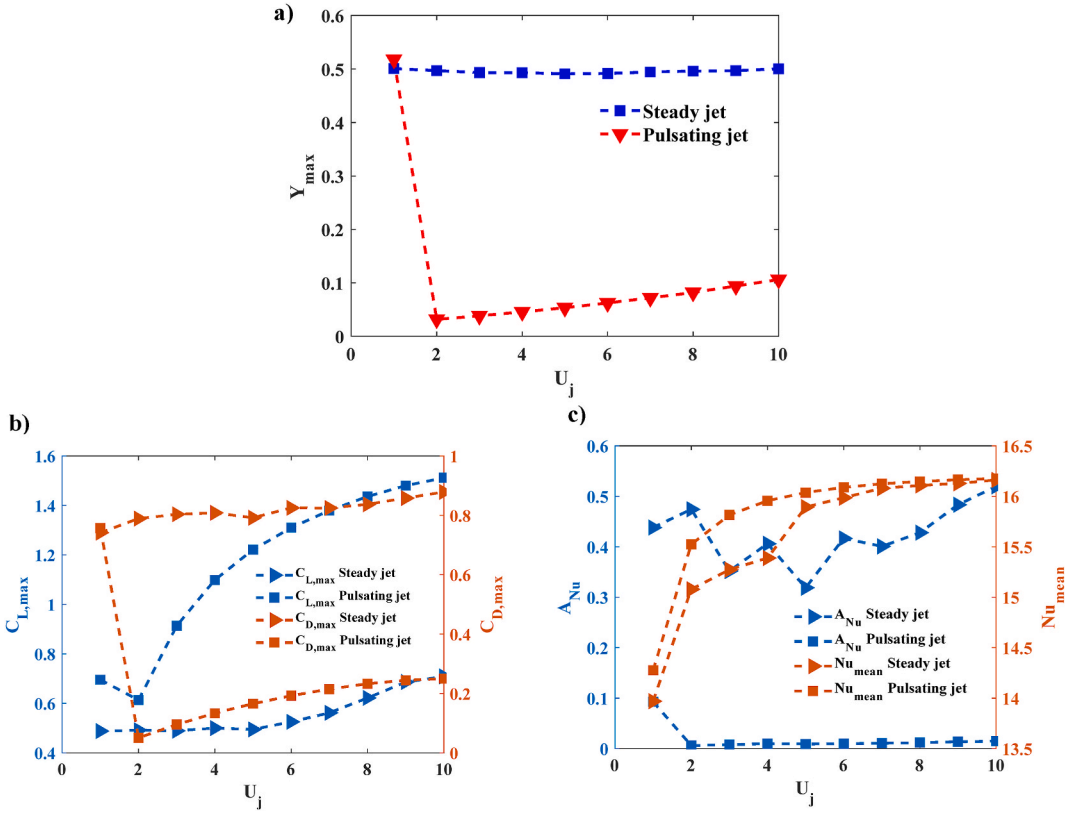

Fig. 6. Changes in the cylinder response for steady and pulsating jet injection from slot 3 in terms of flow injection velocity: a) Maximum displacement, b) Maximum lift and drag coefficients, and c) Amplitude and average of Nusselt number.

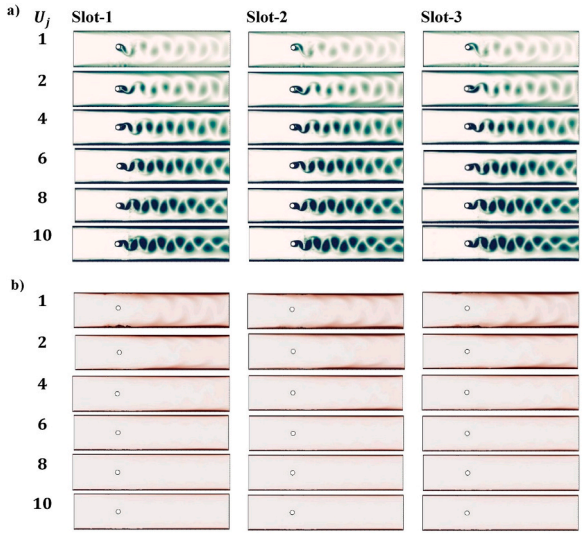

Fig. 7. The variations in a) vortical structure and b) temperature contours in terms of pulsating jet injection velocity from slots 1, 2 and 3.

that the rip-shaped state created next to the channel walls decreases and is eliminated. This indicates that with increasing the jet velocity, the effect of cold and hot fluid mixing has increased, and the average bulk fluid temperature inside the channel has increased.

According to the observed results, the pulsating jet velocity of $U_j = 2$ is an excellent option to be selected as the optimal value for continuing fluid-solid interaction simulations. At this jet velocity, a significant reduction occurred in the cylinder displacement magnitude; keep in mind that the slower the jet velocity, the less energy will also be consumed.

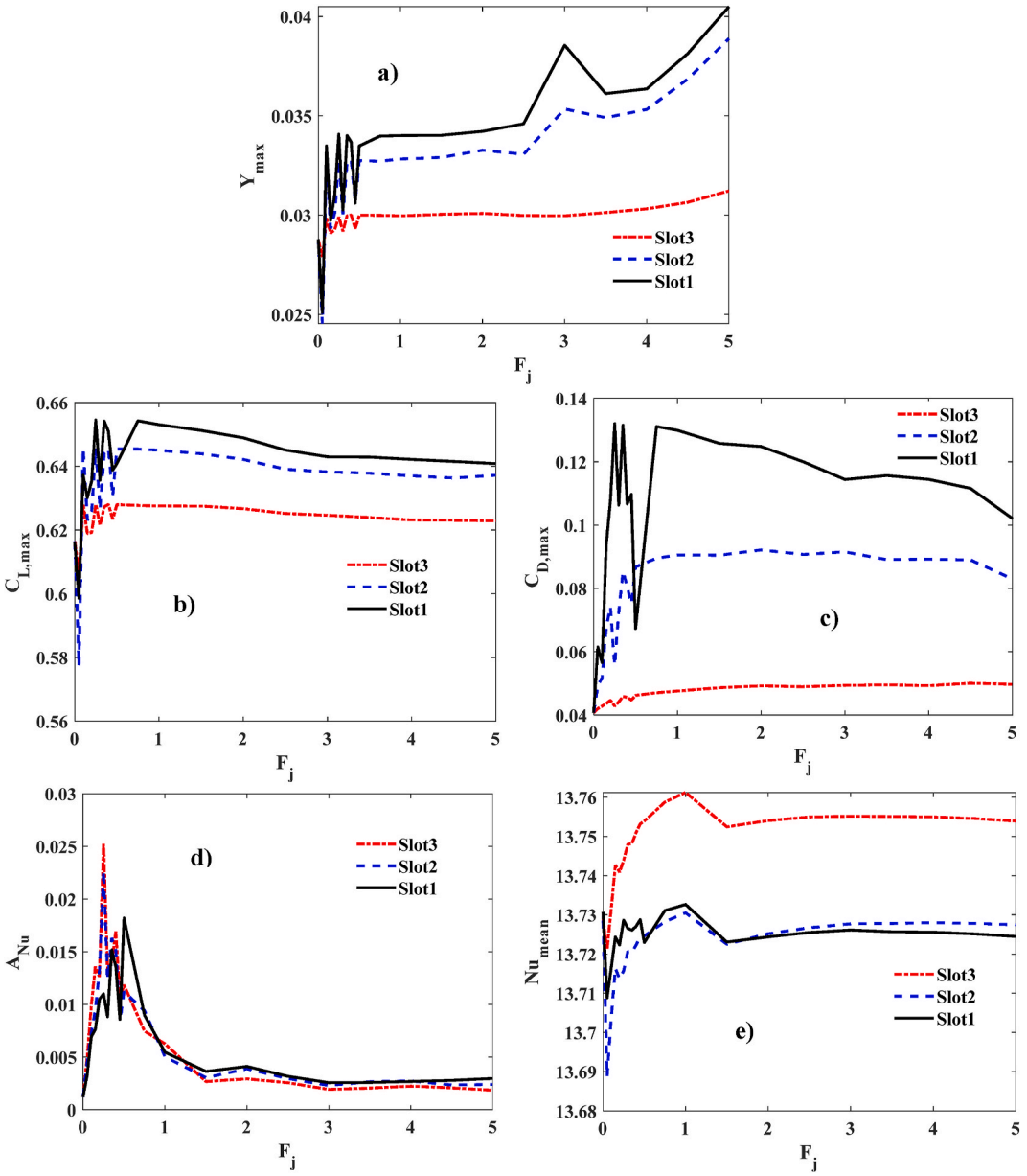

Fig. 8. The change in a) the maximum of displacement magnitude, b) lift and c) drag coefficients, d) amplitude and e) average Nusselt number in terms of pulsating jet frequency for slots 1, 2, and 3.

As a result, in the following, Fig. 8a shows the changes in maximum transverse displacement in terms of pulsating jet frequency ratio for slots 1, 2 and 3 with velocity domain $U_j = 2$ at $Re = 70$. Fig. 8b also shows similar graphs for lift and drag coefficients. It can be seen that at low frequencies ($0.05 < F_j < 0.6$), intermittently changes are observed in the maximum displacement. Then, with increasing frequency in the range of $0.6 < F_j < 2.3$, not much change is seen in the maximum displacement. Then, at higher frequencies ($F_j > 2.3$), the displacement increases, especially for slots closer to the cylinder. In this frequency range, there not much change is seen in displacement for slot 3. Similarly, changes in the maximum of lift and drag coefficients are observed in the low-frequency range. In contrast, as the pulsating jet frequency increases, the lift and drag coefficients decreases.

Fig. 8c shows the change in amplitude and the average of Nusselt number with frequency ratio at $U_j = 2$. The Nusselt number amplitude for all three slots increases with increasing jet frequency to reach its maximum value and then decreases. The maximum amplitude of Nusselt number for slots 1, 2, and 3 are 0.0227, 0.0182, and 0.0252, respectively, which occurred in F_j s of 0.25, 0.5 and 0.25. From $F_j > 2$ the amplitude of the Nusselt number is almost constant. The average Nusselt number also increases and then decreases with increasing jet frequency. From $F_j > 2$, the average of the Nusselt number is almost constant. Almost at F_j equal to 1, the maximum value of the average Nusselt number occurred. It seems that as the jet frequency increases, the fluid inside the channel does

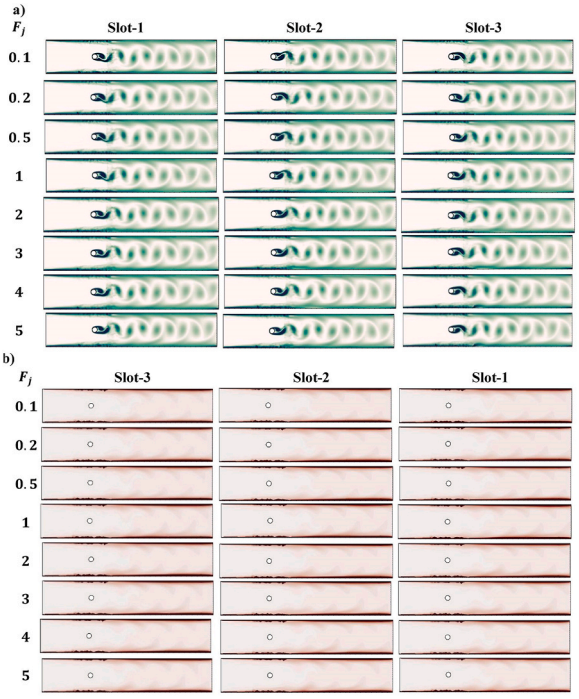

Fig. 9. a) The changes in vorticity contours and b) temperature contours in terms of pulsating jet frequency from slots 1, 2 and 3.

not have the required time to recognize these changes. Therefore, $F_j < 2$ is more effective in changing the amplitude and average of the Nusselt number. According to the observations, it seems that the choice of frequency ratio $F_j = 1$ is a good option because it is far from the range of changes in cylinder response at low frequencies, and also the maximum displacement magnitude is reduced significantly.

Fig. 9a shows the changes in vorticity contours in terms of pulsating jet frequency ratio at $U_j = 2$ for slots 1, 2, and 3. Here, as shown in Fig. 3a, no noticeable change is seen in the vortical structure in the fully-developed condition, and the detectable mode is still the same as 2S. Fig. 9b, in the following, shows the changes in temperature contours in terms of pulsating jet frequency ratio at $U_j = 2$ for slots 1, 2, and 3. A rib-shaped state is seen next to the walls in all shapes. The change of pulsating jet frequency has not affected the temperature pattern in a channel.

In temperature contours, slight changes are observed in the strip shape near the bottom wall of the channel, which is due to the progress of changes caused by vortex shedding and pulsating jet along the channel. The contours also show that as the jet injection site moves away from a cylinder, the average temperature of fluid behind the cylinder decreases slightly.

In the following, the transverse displacement frequency (f_{osc}) in terms of jet injection velocity for slots 1, 2, and 3 is also given for both steady and pulsating jets. It should be noted that the transverse vibration frequency in a non-jet state (uncontrolled cylinder) is equal to $f_{osc} = 0.156$, which is very close to the natural frequency of an oscillator. Due to this frequency matching, the cylinder vibration magnitude has reached its maximum in the lock-in region. It can be seen that the oscillation frequency at low jet velocity $U_j = 1$ is equal to $f_{osc} = 0.158$ for all slots for both pulsating and steady jets. This indicates that jet injection at low velocity has not changed the system vibration frequency. For steady jets, even with the increased flow injection velocity, the cylindrical transverse vibration frequency does not change significantly, and the cylinder remains in the frequency matching region. In the other words, what reduces vibrations due to a steady jet is not changing the oscillations frequency.

In contrast, for pulsating jets, it is seen that the cylinder oscillation frequency increases almost linearly with increasing velocity. Here, by increasing the flow injection velocity of pulsating jets to $U_j = 2$ for all slots, the cylinder is completely exited from the frequency lock-in region, and as a result, the displacement amplitude is drastically reduced. This is why, according to what was seen in Figs. 4–6, apart from injecting jets from the triple slots, the vibration magnitude was significantly reduced at $U_j = 2$. According to what has been explained so far; It is clear that the main reason and mechanism for reducing the cylinder vibration by pulsating jets is to disrupt the frequency matching. In particular, due to flow oscillating action towards the cylinder, the pulsating jet causes significant changes in the vortex shedding frequency that because of it, the oscillator gets out of the frequency matching condition.

Finally, in order to study the reason for the oscillation reduction by steady jets, Fig. 10b shows vorticity contours for several flow injection velocities. As it can be seen, the steady jet reduced the cylinder vibrations by suppressing the vortex shedding at relatively higher injection velocities. Specifically, for $U_j = 3$ from slot 1, it can be seen that the 2S mode has turned into a symmetrical wake. As slot distance from the cylinder increases, the effect of jets on suppressing vortex shedding decreases to the point that for slot 3, the steady jet injection cannot reduce the cylinder vibrations.

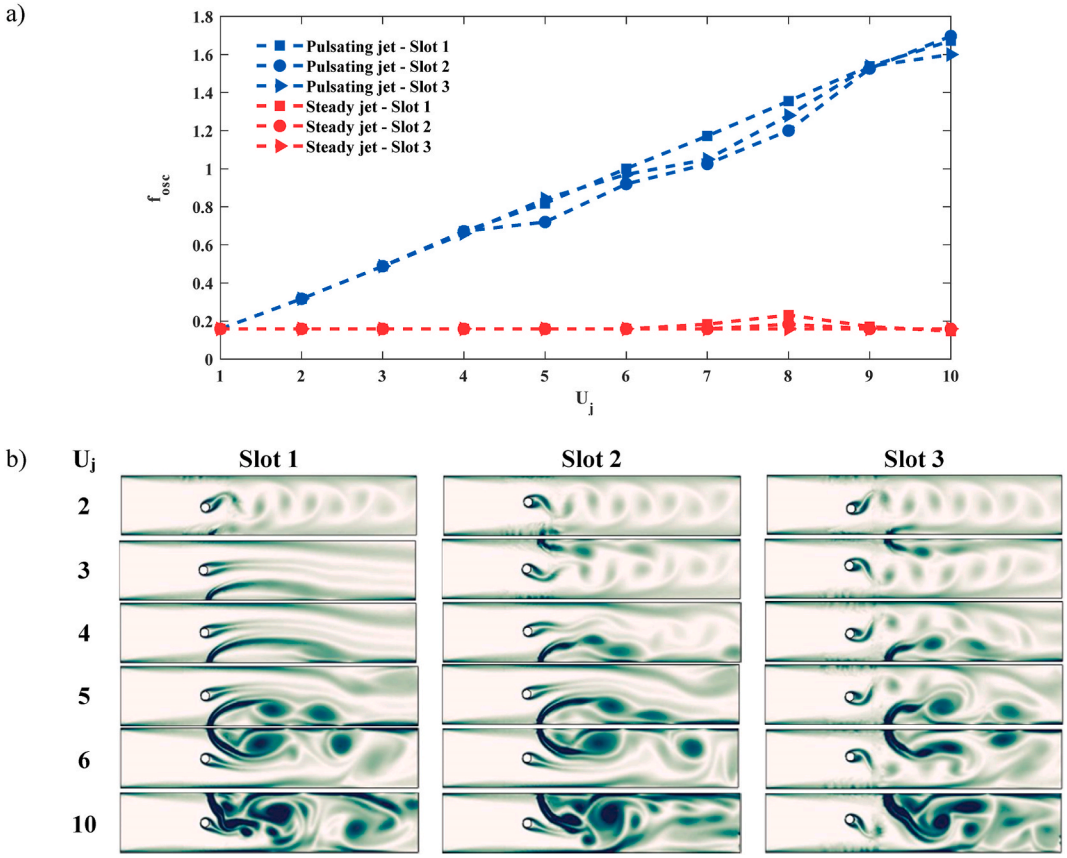

Fig. 10. a) The changes in transverse vibration frequency and b) The changes in the vortical structure in terms of injection velocity of steady and pulsating jets from slots 1, 2 and 3.

6. Conclusion

In the present paper, the effect of steady and oscillating jets on the vibrational and thermal behavior of a sprung cylinder as well as vorticity and temperature contours, are taken into account. An elastically-mounted circular cylinder is placed inside a channel. The most important results obtained are as follows:

1) The distance of the jet slot from the cylinder is very important in reducing VIV, and the steady jet of slot 3 cannot reduce the VIV at any injection velocity. For pulsating jets, similar behavior is observed in all slots: a significant decrease in the displacement domain at $U_j = 2$ and then a gradual and slight increase in displacement with increasing pulsating jet velocity. As a result, it can be said that the pulsating jet velocity has a more significant effect on the displacement reduction than the frequency.
2) The average Nusselt number in the steady and pulsating jets is higher than the non-jet case. The average Nusselt number of pulsating jets is more heightened than steady ones. When the pulsating jet frequency is 1, the maximum Nusselt number is obtained.
3) The pulsating jet has no significant effect on the vorticity structure, and the vortex shedding mode is the same as the classic 2S mode. The primary mechanism to reduce vibrations in steady jets is suppressing the vortex shedding (direct effect in cylinder wake). The main mechanism to reduce vibrations in pulsating jets is to change the vortex shedding frequency. As a result, the cylinder gets out of the lock-in region and the VIV is reduced independently of jet injection from the triple slots. The findings of the present study can be used to improve the design and construction of heat exchangers and solar air heaters to increase efficiency and reduce structural vibrations.

Author statement

S.D. Farahani: analysis and/or interpretation of data. A.H. Rabiee: Conception and design of study, Drafting the manuscript. A.M. Zakinia: acquisition of data. A.H. Mosavi: analysis and/or interpretation of data.

Declaration of competing interest

The authors declare that they have no known competing financial interests or personal relationships that could have appeared to influence the work reported in this paper.

References

[1] P. Dey, Optimal position of square cylinder vortex generator in channel is not a function of ordinate only–A heat transfer and optimization study, Engineering Science and Technology, Int. J. (2021).
[2] P. Dey, A.K. Das, Numerical analysis of drag and lift reduction of square cylinder, Engineering Science and Technology, Int. J. 18 (4) (2015) 758–768.
[3] R. Gabbai, H. Benaroya, An overview of modeling and experiments of vortex-induced vibration of circular cylinders, J. Sound Vib. 282 (3–5) (2005) 575–616.
[4] J. Shi, J. Hu, S.R. Schafer, C.-L.C. Chen, Numerical study of heat transfer enhancement of channel via vortex-induced vibration, Appl. Therm. Eng. 70 (1) (2014) 838–845.
[5] A.H. Rabiee, S. Farahani, A comprehensive study of heat transfer characteristic and two-dimensional FIV for heated square-section cylinder with different damping ratios, Int. Commun. Heat Mass Tran. 116 (2020) 104680.
[6] A. Rabiee, M. Barzan, A. Mohammadebrahim, Flow-induced vibration suppression of elastic square cylinder using windward-suction-leeward-blowing approach, Appl. Ocean Res. 109 (2021) 102552.
[7] S. Farahani, A.H. Rabiee, Transverse FIV suppression of square cylinder using two control rods of varying size and distance in lock-in and galloping regions, Int. J. Numer. Methods Heat Fluid Flow (2021).
[8] M. Esmaeili, A.H. Rabiee, Active feedback VIV control of sprung circular cylinder using TDE-iPID control strategy at moderate Reynolds numbers, Int. J. Mech. Sci. 202 (2021) 106515.
[9] M. Sarmeili, H.R. Ashtiani, A. Rabiee, Nonlinear energy sinks with nonlinear control strategies in fluid-structure simulations framework for passive and active FIV control of sprung cylinders, Commun. Nonlinear Sci. Numer. Simulat. 97 (2021) 105725.
[10] J. Sui, J. Wang, S. Liang, Q. Tian, VIV suppression for a large mass-damping cylinder attached with helical strakes, J. Fluid Struct. 62 (2016) 125–146.
[11] M. Lou, Z. Chen, P. Chen, Experimental investigation of the suppression of vortex induced vibration of two interfering risers with splitter plates, J. Nat. Gas Sci. Eng. 35 (2016) 736–752.
[12] A.H. Rabiee, M. Esmaeili, The effect of externally applied rotational oscillations on FIV characteristics of tandem circular cylinders for different spacing ratios, Int. J. Numer. Methods Heat Fluid Flow (2020).
[13] A.H. Rabiee, Galloping and VIV control of square-section cylinder utilizing direct opposing smart control force, J. Theor. Appl. Vib. Acoust. 5 (1) (2019) 69–84.
[14] D.R. Williams, H. Mansy, C. Amato, The response and symmetry properties of a cylinder wake subjected to localized surface excitation, J. Fluid Mech. 234 (1992) 71–96.
[15] L.H. Feng, J.J. Wang, Circular cylinder vortex-synchronization control with a synthetic jet positioned at the rear stagnation point, J. Fluid Mech. 662 (2010) 232.
[16] L.-H. Feng, J.-J. Wang, Modification of a circular cylinder wake with synthetic jet: vortex shedding modes and mechanism, Eur. J. Mech. B Fluid 43 (2014) 14–32.
[17] S. Dong, G. Triantafyllou, G. Karniadakis, Elimination of vortex streets in bluff-body flows, Phys. Rev. Lett. 100 (20) (2008) 204501.
[18] W.-L. Chen, X. Wang, F. Xu, H. Li, H. Hu, Passive jet flow control method for suppressing unsteady vortex shedding from a circular cylinder, J. Aero. Eng. 30 (1) (2017), 04016063.
[19] H. Wang, L. Ding, L. Zhang, Q. Zou, R.N. Sharma, Control of two-degree-of-freedom vortex induced vibrations of a circular cylinder using synthetic Jets: effect of synthetic jet orientation angle and phase difference, Ocean Eng. 217 (2020) 107906.
[20] H. Malah, Y.S. Chumakov, E. Sadeghian, The effects of the cross-section shape of the surface-mounted cylinder on the free convective junction flow, Engineering Science and Technology, Int. J. (2021).
[21] F. Selimefendigil, H.F. Öztop, Mixed convection of ferrofluids in a lid driven cavity with two rotating cylinders, Engineering Science and Technology, Int. J. 18 (3) (2015) 439–451.
[22] L. Baranyi, Computation of unsteady momentum and heat transfer from a fixed circular cylinder in laminar flow, J. Comput. Appl. Mech. 4 (1) (2003) 13–25.
[23] A. Kumar, A. Dhiman, L. Baranyi, Fluid flow and heat transfer around a confined semi-circular cylinder: onset of vortex shedding and effects of Reynolds and Prandtl numbers, Int. J. Heat Mass Tran. 102 (2016) 417–425.
[24] N. Sharma, A.K. Dhiman, S. Kumar, Mixed convection flow and heat transfer across a square cylinder under the influence of aiding buoyancy at low Reynolds numbers, Int. J. Heat Mass Tran. 55 (9–10) (2012) 2601–2614.
[25] A. Dhiman, M. Hasan, Flow and heat transfer over a trapezoidal cylinder: steady and unsteady regimes, Asia Pac. J. Chem. Eng. 8 (3) (2013) 433–446.
[26] A.K. Dhiman, Flow and heat transfer phenomena around an equilateral triangular bluff body: effect of wall confinement, Heat Tran. Asian Res. 45 (7) (2016) 608–630.
[27] D. Chatterjee, S. Amiroudine, Two-dimensional mixed convection heat transfer from confined tandem square cylinders in cross-flow at low Reynolds numbers, Int. Commun. Heat Mass Tran. 37 (1) (2010) 7–16.
[28] W. Lin, Z.B. Chen, J.Y. Yu, X.T. Zheng, Analysis of vortex-induced vibration and heat transfer of an elastic cylinder at low Reynolds numbers, in: Applied Mechanics and Materials, Trans Tech Publ, 2014, pp. 458–464.
[29] Y. Su, L. Gao, L. Li, X. Li, C. Zhang, A study of the vortex-induced lateral vibration and heat transfer characteristics of elastic supported single tubes with different cross-sectional shapes, Int. Commun. Heat Mass Tran. 104 (2019) 8–14.
[30] E. Izadpanah, Y. Amini, A. Ashouri, A comprehensive investigation of vortex induced vibration effects on the heat transfer from a circular cylinder, Int. J. Therm. Sci. 125 (2018) 405–418.
[31] Z. Yang, L. Ding, L. Zhang, L. Yang, H. He, Two degrees of freedom flow-induced vibration and heat transfer of an isothermal cylinder, Int. J. Heat Mass Tran. 154 (2020) 119766.
[32] A.H. Rabiee, S.D. Farahani, Effect of synthetic jet on VIV and heat transfer behavior of heated sprung circular cylinder embedded in a channel, Int. Commun. Heat Mass Tran. 119 (2020) 104977.
[33] T. Prasanth, S. Mittal, Vortex-induced vibrations of a circular cylinder at low Reynolds numbers, J. Fluid Mech. 594 (2008) 463–491.
[34] S. Singha, K. Sinhamahapatra, Flow past a circular cylinder between parallel walls at low Reynolds numbers, Ocean Eng. 37 (8–9) (2010) 757–769.
[35] W. Khan, J. Culham, M. Yovanovich, Fluid flow and heat transfer from a cylinder between parallel planes, J. Thermophys. Heat Tran. 18 (3) (2004) 395–403.